

Article

Design and Characterization of Nanostructured Titanium Monoxide Films Decorated with Polyaniline Species

Tomas Sabirovas ¹, Simonas Ramanavicius ^{1,*}, Arnas Naujokaitis ², Gediminas Niaura ³ and Arunas Jagminas ^{1,*}

¹ State Research Institute Centre for Physical Sciences and Technology, Department of Electrochemical Material Science, Sauletekio Ave. 3, LT-10257 Vilnius, Lithuania

² State Research Institute Centre for Physical Sciences and Technology, Department of Characterization of Materials Structure, Sauletekio Ave. 3, LT-10257 Vilnius, Lithuania

³ State Research Institute Centre for Physical Sciences and Technology, Department of Organic Chemistry, Sauletekio Ave. 3, LT-10257 Vilnius, Lithuania

* Correspondence: simonas.ramanavicius@ftmc.lt (S.R.); arunas.jagminas@ftmc.lt (A.J.)

Abstract: The fabrication of nanostructured composite materials is an active field of materials chemistry. However, the ensembles of nanostructured titanium monoxide and suboxide species decorated with polyaniline (PANI) species have not been deeply investigated up to now. In this study, such composites were formed on both hydrothermally oxidized and anodized Ti substrates via oxidative polymerization of aniline. In this way, highly porous nanotube-shaped titanium dioxide (TiO₂) and nano leaflet-shaped titanium monoxide (TiO_x) species films loaded with electrically conductive PANI in an emeraldine salt form were designed. Apart from compositional and structural characterization with Field Emission Scanning Electron Microscopy (FESEM) and Raman techniques, the electrochemical properties were identified for each layer using cyclic voltammetry and electrochemical impedance spectroscopy (EIS). Based on the experimentally determined EIS parameters, it is envisaged that TiO-based nanomaterials decorated with PANI could find prospective applications in supercapacitors and biosensing.

Keywords: polyaniline; titanium; monoxide; titanium dioxide; oxidative polymerization; anodizing; electrochemical impedance spectroscopy



Citation: Sabirovas, T.; Ramanavicius, S.; Naujokaitis, A.; Niaura, G.; Jagminas, A. Design and Characterization of Nanostructured Titanium Monoxide Films Decorated with Polyaniline Species. *Coatings* **2022**, *12*, 1615. <https://doi.org/10.3390/coatings12111615>

Academic Editor: Maria Vittoria Diamanti

Received: 30 September 2022

Accepted: 20 October 2022

Published: 24 October 2022

Publisher's Note: MDPI stays neutral with regard to jurisdictional claims in published maps and institutional affiliations.



Copyright: © 2022 by the authors. Licensee MDPI, Basel, Switzerland. This article is an open access article distributed under the terms and conditions of the Creative Commons Attribution (CC BY) license (<https://creativecommons.org/licenses/by/4.0/>).

1. Introduction

Electrically conducting polymers are promising alternative materials for technological applications in many areas, including chemistry, material sciences, and engineering [1,2]. Conducting polymers-based nanocomposites also have outstanding potential applications in biomedical fields [3], such as antimicrobial therapy [4], drug delivery [5], wearable energy harvesting devices [6], nerve regeneration [7], and tissue engineering [8]. Conducting polymers are also frequently applied in the design of supercapacitors [9]. Modification of metal oxides by conducting polymers significantly improves electrochemical capacitance [10]. Capacity variations of conducting polymer-based structures can be well applied in various conducting-polymer-based sensors [11] and biosensors [12]. Due to its high electrical conductivity, biocompatibility, low toxicity, and good environmental stability, polyaniline (PANI) is one of the most studied conducting polymers [13]. Three redox forms of polyaniline are usually distinguished: leucoemeraldine (reduced), emeraldine (half-oxidized), and pernigraniline (fully oxidized), differing in color and electrical conductivity [14,15]. Traditionally, PANI layers are designed onto various substrates by electrochemical treatment in acidic solutions containing aniline. PANI can also be synthesized by chemical oxidative polymerization (COP) of aniline monomer using ammonium persulfate as a redox initiator [16]. However, to the extent of the authors' knowledge, only a few reports have covered titanium monoxide and suboxide structures with PANI at the time of this writing [17,18],

whereas none of them investigated nanostructures or nanostructured surfaces as it is done in this study.

There is a variety of applications for titania [19], but for titanium suboxides, despite their advantageous properties such as high electrical conductivity and low bandgap [20], application areas are still not clear. Up to now, several publications have reported on titanium–suboxides-based gas sensors [21,22], microbial fuel cells [18], substrates for electrocatalysts [23], solar cells [24], optoelectronic devices [25], batteries [26], etc. While many common synthesis methods exist for TiO_2 , such as anodization [27], microwave synthesis [28], laser beam treating [29] and chemical oxidation [30], these methods are not suitable for the formation of nonstoichiometric titanium oxide structures. One of the well-known approaches for the formation of titanium suboxide materials is the reduction of TiO_2 by heating in an H_2 atmosphere, with TiH_4 , NaBH_4 , Al, Mg, either with Zn powder [31–33]. Note that the presence of oxygen vacancy, Ti^{3+} and Ti-OH in titanium monoxides and suboxides contributed to their high photocatalytic efficiency and significantly lower band gaps [20]. However, these processes require lengthy processing at high temperatures in a vacuum, and both structure size and surface morphology are difficult to control [34]. Therefore, in this study, we designed the chemical oxidation of the Ti surface into titanium suboxide thin films by hydrothermal treatment under appropriate oxidation/dissolution reactivity with a controllable thickness and surface morphology. For this, an alkaline solution of $0.4 \text{ mol L}^{-1} \text{H}_2\text{SeO}_3$, already reported by us [35], has been slightly modified and used in this study. In this way, highly porous nanostructured films composed of titanium monoxide, TiO_x , species possessing a low band gap (1.29 eV) value and hierarchical morphology have been prepared.

The aim of this study is the formation of nanoplatelet titanium monoxide films decorated with polyaniline (PANI) for application as a supercapacitor. Decorated titanium monoxide film surface morphology was investigated by FESEM, the formation of PANI in Emeraldine form was proved by Raman spectroscopy, whereas cyclic voltammetry and electrochemical impedance spectroscopy were applied for the investigation of capacitive properties. Moreover, for purposes of comparison, PANI deposited onto anodized Ti substrates was investigated in this study.

2. Materials and Methods

2.1. Synthesis and Characterization

Analytical grade ammonium fluoride, sodium hydroxide, potassium peroxydisulfate, $\text{K}_2\text{S}_2\text{O}_8$, acids: HCl , H_3PO_4 , HClO_4 , H_2SeO_3 , and aniline purchased from Sigma-Aldrich were used for the preparation of aqueous solutions. The 99.7% purity Ti working samples in dimensions of $10 \times 10 \text{ mm}^2$ were cut from a Ti foil, 0.127 mm thick (Sigma-Aldrich, Taufkirchen, Germany). The samples were ultrasonically cleaned by sonication in acetone, ethanol and water baths, 6 min each. An aqueous solution containing $2 \text{ mol L}^{-1} \text{H}_3\text{PO}_4$ and $0.3 \text{ mol L}^{-1} \text{NH}_4\text{F}$ was applied for Ti nanoporous anodizing at 20 V for 2 h., whereas chemical oxidation of Ti foil was performed by hydrothermal treatment in an alkaline solution of $0.3 \text{ mol L}^{-1} \text{H}_2\text{SeO}_3$ and NaOH at 150–200 °C for 15 h., as previously reported by us [35], followed by rigorous rinsing. To obtain a denser and thicker layer compared to the previous study, the pH of the solution was increased to 10.0 and the temperature of autoclaving to 200 °C. Prior to further depositions, all samples were annealed in argon at 350 °C for 2 h. Similar to the methodology reported by Rahman et al. [36], an aqueous solution of HCl , aniline and potassium peroxydisulfate ($\text{K}_2\text{S}_2\text{O}_8$) was used for the chemical deposition of polyaniline. For this purpose, 0.02 mL aniline was dissolved under vigorous stirring in 22 mL $1.0 \text{ mol L}^{-1} \text{HCl}$ solution at the ice temperature. Then, 2 mL of a solution containing $25 \text{ mg mL}^{-1} \text{K}_2\text{S}_2\text{O}_8$ salt also kept at ice temperature was added dropwise under intense stirring, then the Ti sample was inserted in the mixture and kept from 12 to 48 h. Finally, the sample was washed with water several times, dried at 60 °C, and stored in a desiccator for characterization. SEM images were obtained using the Helios Nanolab 650 field emission scanning electron microscope (FEI Eindhoven, The Netherlands).

2.2. Raman Spectroscopy

A Renishaw InVia spectrometer (Wotton-under-Edge, UK) equipped with a thermoelectrically cooled ($-70\text{ }^{\circ}\text{C}$) CCD camera and a microscope was used for Raman spectroscopy measurements. Raman spectra were excited with 632.8 nm radiation from a He-Ne gas laser. The $20\times/0.40$ NA objective lens and 1800 lines/mm grating was used, where the accumulation time of Raman spectra was 400 s. The power of the laser was decreased to 0.3 mW to avoid possible destruction of the samples. The polystyrene standard spectrum was used to calibrate the Raman scattering wavenumber axis. Experimental data were fitted with Gaussian-Lorentzian shape components using GRAMS/A1 8.0 (Thermo Scientific, Waltham, MA, USA) software to determine the parameters of the bands.

2.3. Electrochemical Measurements

Electrochemical measurements of cyclic voltammetry and electrochemical impedance spectroscopy were carried out using an electrochemical workstation Zahner Zennium (Kronach, Germany) in a standard three-electrode cell with the working electrode, Ag/AgCl_{sat} reference electrode, and platinum (99.99% purity, Aldrich) wire as a counter electrode. As a working electrode, pristine substrates and PANI-decorated substrates (12 h incubation time) were selected. Electrochemical impedance spectroscopy (EIS) was conducted in a frequency range of 0.1 Hz– 10^5 Hz with 10 mV amplitude. The data were normalized to the surface area of the electrodes (0.16 cm^2). Multiple experiments (up to 5) were carried out to account for data discrepancy.

3. Results

3.1. Structural Characterization

Hydrothermal treatment of titanium in strongly alkaline solutions at $150\text{--}200\text{ }^{\circ}\text{C}$ results in its surface etching and oxidation covering by densely packed crystallite grains (Figure 1A). The average size of titanium hydrate species varied from several to several tens of nanometers, depending on the processing conditions, such as the solution pH, temperature, and treatment duration. The subsequent calcination of this ensemble at $300\text{--}350\text{ }^{\circ}\text{C}$ in air results in titanium hydrate crystallization to TiO₂ [37,38].

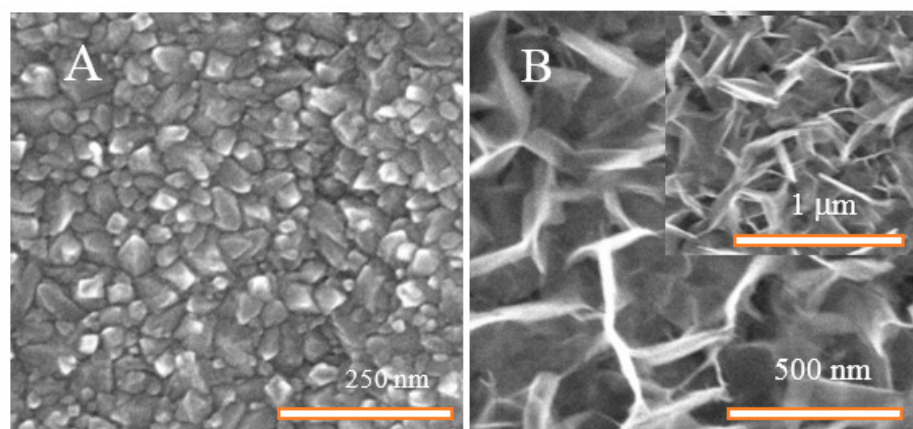


Figure 1. Top-side SEM images of the Ti surface after hydrothermal treatment in the solution of NaOH (pH = 11.0) at $150\text{ }^{\circ}\text{C}$ for 15 h (A) and $0.3\text{ mol L}^{-1}\text{ H}_2\text{SeO}_3 + \text{NaOH}$ solution (pH = 10.0) at $150\text{ }^{\circ}\text{C}$ (B).

However, variations in the hydrothermal treatment conditions and pH did not allow us to form nanostructured titanium monoxide or suboxide films. Therefore, in this study, we applied the hydrothermal processing in an aqueous alkaline solution containing SeO_3^{2-} , which upon a slow hydrolysis reaction at high temperature and pressure produces reactive OH^- species and TiOH [35]. Long-time hydrothermal treatment of a Ti substrate in this solution even at $150\text{ }^{\circ}\text{C}$ resulted in the formation of a thin ($\cong 1.0\text{ }\mu\text{m}$) layer comprising a

leaflet-type species array (Figure 1B). The rise in the autoclave temperature to 200 °C results in the formation of thicker films of the more densely packed and needle-shaped leaflets with lateral dimensions of 8–13 nm \times 0.5–1.1 μ m (Figure 2A). The SEM images shown in the Figure 2B–D panels imply that the entire surface of all TiO_x needle-shaped leaflets is decorated with frost-type precipitates after prolonged sonication of the TiO_x in the cold aniline solution with potassium persulfate. Upon vigorous mixing for 12, 24, and 48 h, the initial thickness of TiO_x needles increased to 50–60 nm, 150–170 nm, and 200–250 nm, respectively, although the porous morphology of the film was preserved even after 48 h of processing. From the previous research, after calcination in an oxygen-free atmosphere, these leaflets comprise titanium monoxide [35].

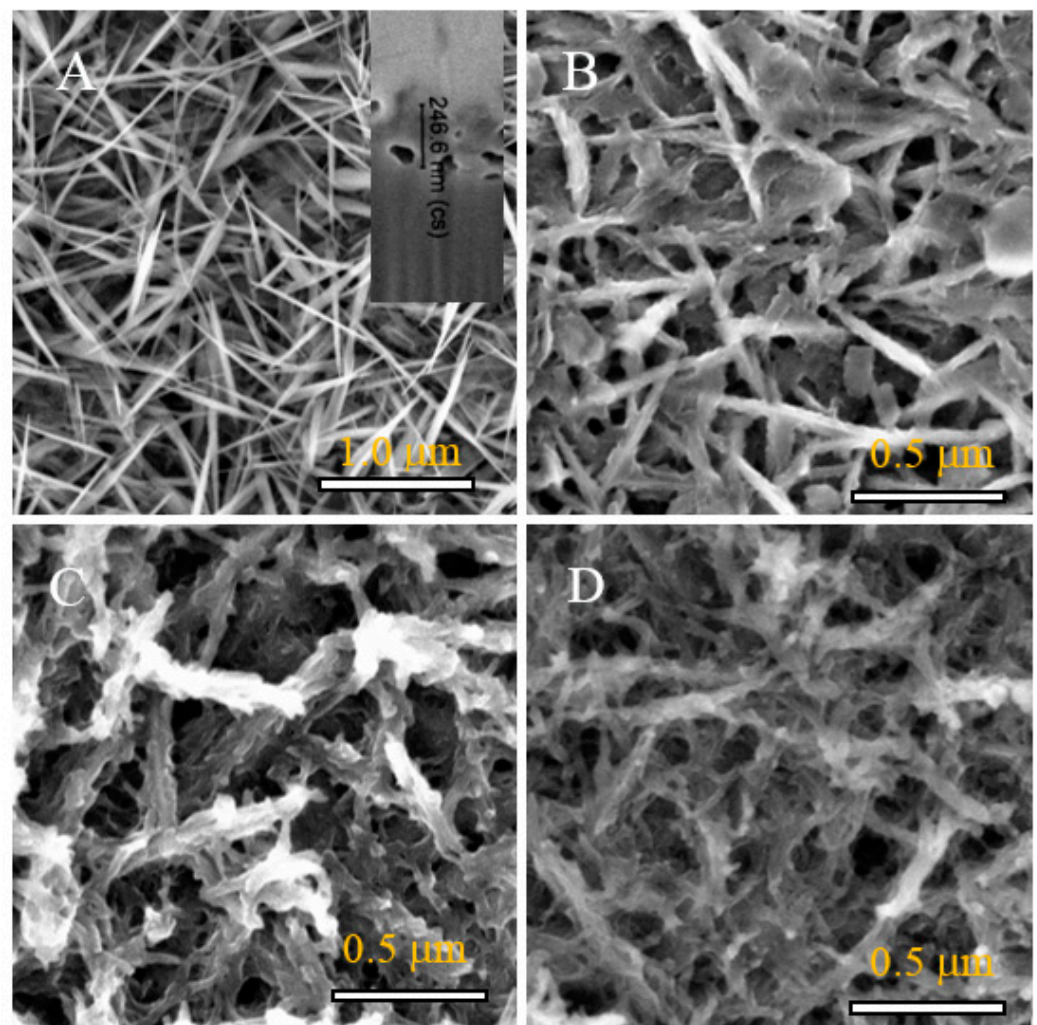


Figure 2. Top-side FESEM images of TiO_x film before (A) and after (B–D) covering with polyaniline by chemical oxidation of aniline with potassium persulfate at 2–4 °C for 12 (B), 24 (C), and 48 h. (D). The inset shows the film thickness of film grown at 200 °C for 15 h: pH = 10; 0.3 M SeO₃^{2−}.

For purposes of comparison, we also prepared Ti samples covered with porous anodic oxide film sandwiched with PANI, focusing on the relation between structure and electrochemical properties between these layers. The Ti surface was prepared by anodizing in an aqueous solution containing 2.0 mol L^{−1} H₃PO₄ and 0.2 mol L^{−1} NH₄F at 20 V for 3 h and subsequent oxidation of aniline with K₂S₂O₈ at ice temperature for 12 h. The aniline–K₂S₂O₈ solution was found to greatly influence the microstructure of PANI species deposited on the nanotubed anatase TiO₂ surface (Figure 3). We established that formation of polymer species on the TiO₂ substrate by chemical oxidation of aniline proceeds easily and required no surface pretreatment, as reported previously [39]. Furthermore, the mor-

phology of as-formed species onto the TiO_2 surface differs significantly from the frost-type precipitates decorated on the TiO_x leaflets (Figure 3).

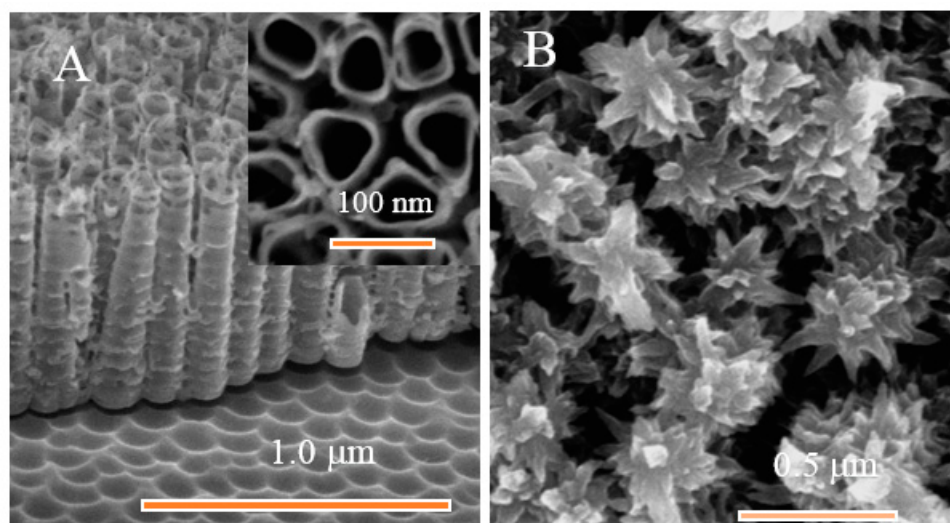


Figure 3. Panoramic (A) and top-side [inset in (A)] SEM image of TiO_2 film before and after polyaniline chemical deposition (B) from an aqueous solution of 1 mol L^{-1} HCl containing 0.9 mL L^{-1} aniline and 90 mL L^{-1} $\text{K}_2\text{S}_2\text{O}_8$ solution (2.5 wt.%) at ice temperature for 12 h.

3.2. Raman Spectroscopy

Resonance Raman spectroscopy provides rich molecular level information on the structure, oxidation and protonation states of polyaniline (PANI) [14,40–44]. Figure 4 compares 632.8-nm excited Raman spectra of $\text{Ti/TiO}_x/\text{PANI}$ and $\text{Ti/TiO}_2/\text{PANI}$ samples. Two strong bands at 1169 and 1589 cm^{-1} belong to C–H bending and C=C stretching vibrations of quinone rings, respectively, whereas the broad feature at 1487 cm^{-1} is associated with C=N stretching vibration of an emeraldine base (imine sites) [14,40]. The shoulder near 1618 cm^{-1} is related to the stretching vibration of the benzene ring. Both samples exhibit a strong band near 1339 cm^{-1} which was assigned to stretching vibration of polaronic structures $\text{C}\sim\text{N}^+$ possessing a bond intermediate between the single and double bonds [43]. These structures are responsible for the conductivity of the film. The middle-intensity feature near 812 cm^{-1} is related to C–N–C bending motion [14], whereas well-defined bands at 521 and 428 cm^{-1} are associated with amine group in-plane deformation and ring deformation modes [14,40]. The sharp band at 579 cm^{-1} was previously assigned to the presence of phenazine-like crosslinked structures in the film [44,45]. Such structures are usually synthesized during the annealing procedure at higher temperatures. The amount of such structures is higher in the case of TiO_x/PANI film. The low-intensity band at 1223 cm^{-1} is characteristic of the C–N stretching mode of emeraldine (amine sites) [14].

In general, the spectral pattern shown in Figure 4 indicates that the polyaniline films are in the emeraldine structure. A relatively intense polaron band at 1339 cm^{-1} evidences the presence of conductive emeraldine salt form in the films. However, because the relative intensity of the polaronic band is higher for the sample $\text{Ti/TiO}_x/\text{PANI}$, this sample should possess higher conductivity. In addition, it should be noted that sample $\text{Ti/TiO}_x/\text{PANI}$ contains a higher number of phenazine-like structures.

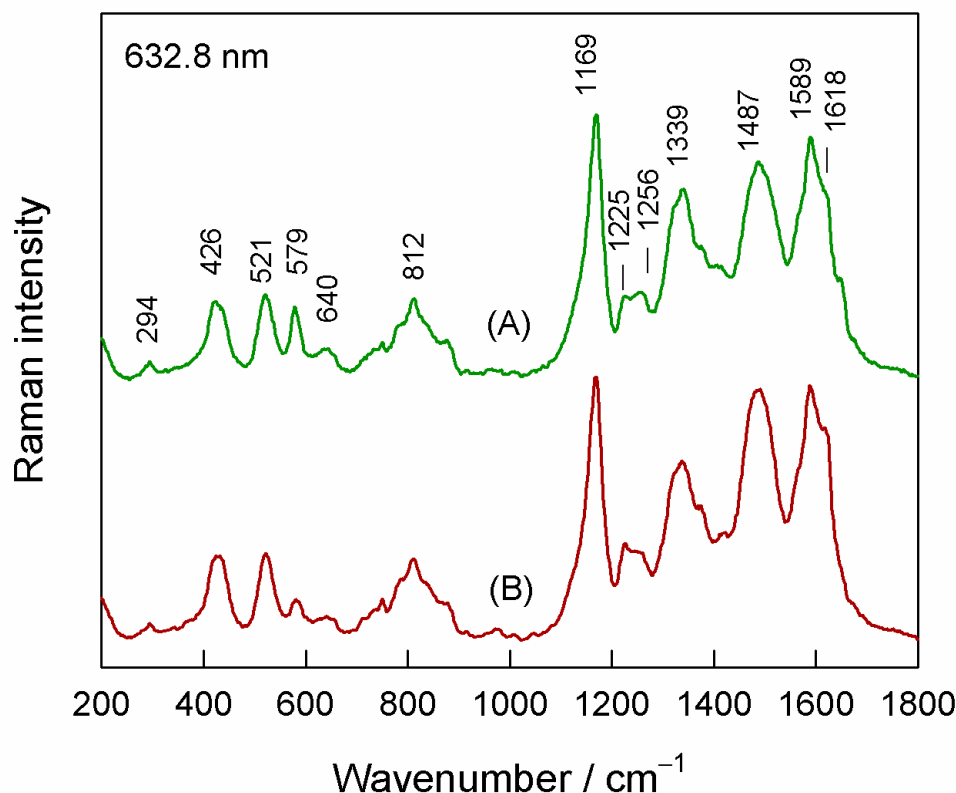


Figure 4. Raman spectrum of (A)–Ti/TiO_x/PANI sample and (B) Ti/TiO₂/PANI sample. Excitation wavelength 632.8 nm (0.1 mW).

3.3. Electrochemical Analysis

Cyclic voltammetry and electrochemical impedance spectroscopy techniques were used to elucidate the electrochemical properties of Ti/TiO_x and Ti/TiO₂ electrodes before and after samples were decorated with PANI. Both Ti/TiO₂ and Ti/TiO₂/PANI samples exhibited oxidation and reduction peaks upon injection of a redox probe (Figure 5A,C). However, different redox reaction responses were observed among Ti/TiO₂ and Ti/TiO₂/PANI samples. First, the peak-to-peak potential separation value (ΔE_p) of the [Fe(CN)₆]^{3−}/[Fe(CN)₆]^{4−} redox pair (Figure 5A,C) on the Ti/TiO₂ sample decreased from 1020 mV to 100 mV when nanotubed TiO₂ film was decorated with PANI, a tenfold difference, implying a significant acceleration of the electron-transfer process. Secondly, in the presence of a redox probe, the PANI-decorated Ti/TiO₂ specimens also exhibited significantly higher anodic and cathodic peak currents.

Contrary to Ti/TiO₂ samples, no distinct oxidation and reduction peaks were observed in the presence of a redox probe for the Ti/TiO_x sample (Figure 5B). Furthermore, the peak-to-peak potential separation value for Ti/TiO_x was estimated to be $\Delta E_p \sim 1500$ mV, which is significantly higher than the value observed for the Ti/TiO₂ electrode, indicating that electron-transfer kinetics are much slower due to the presence of a titanium monoxide barrier. After decoration of TiO_x leaflets with PANI, an obvious enhancement of redox reaction was observed (Figure 5D). The Ti/TiO_x electrode decorated with PANI displayed significantly lower ΔE_p value of 150 mV compared to ΔE_p of 1500 mV obtained for Ti/TiO_x electrodes. Notably, both electrodes, i.e., Ti/TiO_x/PANI and Ti/TiO₂/PANI, display redox reaction peaks, which are located at the potential associated with the transition of PANI forms between leucoemeraldine and emeraldine (A₁ and A₂) and of by-products, namely, hydroquinine/benzoquinone redox reaction (B₁ and B₂) [46,47].

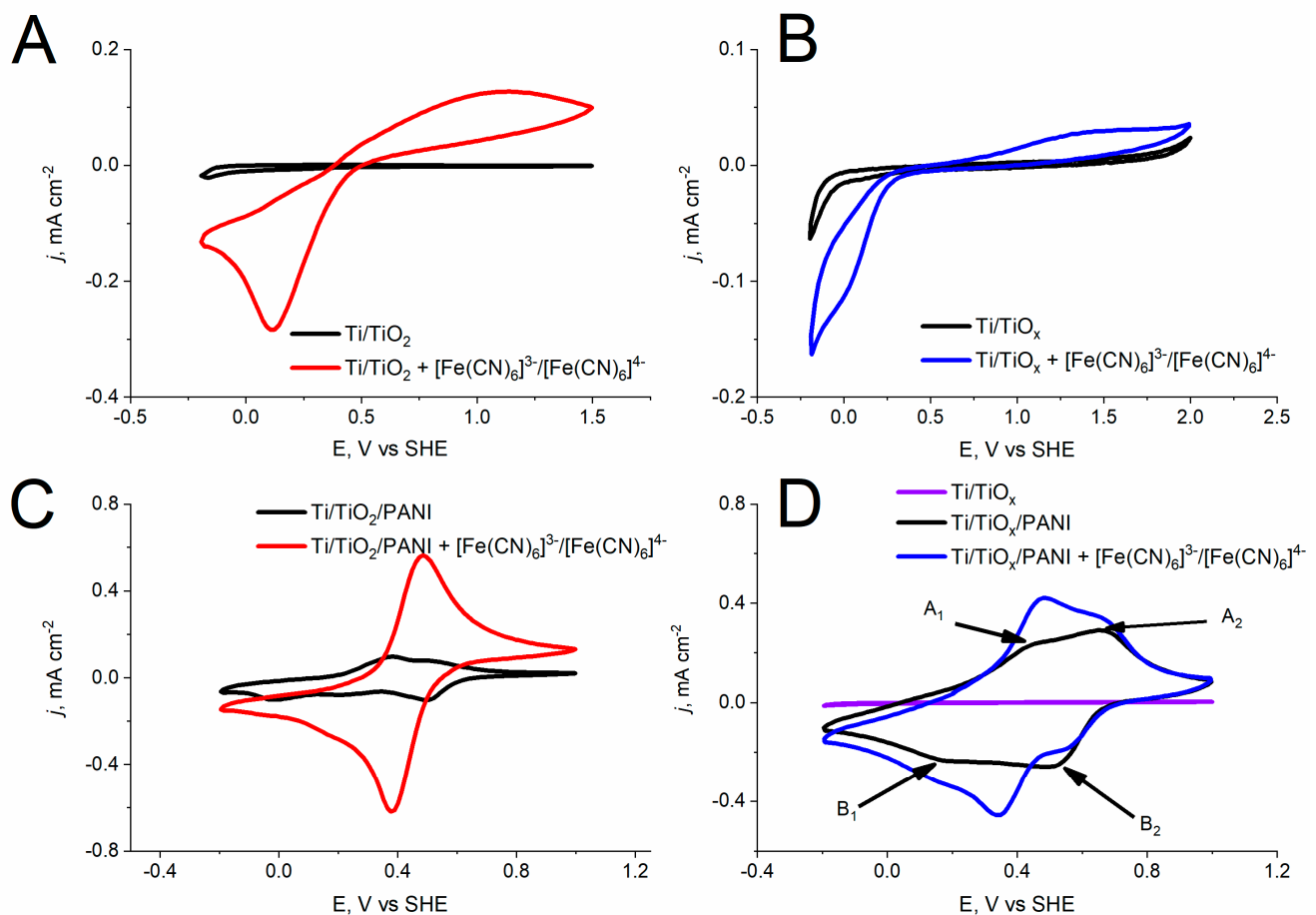


Figure 5. Nyquist plots of Ti/TiO₂, Ti/TiO₂/PANI (A) and TiO_x, TiO_x/PANI (B) with and without (C,D) 5 mM [Fe(CN)₆]^{3−}/[Fe(CN)₆]^{4−} in 0.5 M HCl (pH = 3) solution. Scan rate: 10 mV s^{−1}.

Electrochemical properties of PANI-decorated Ti/TiO_x and Ti/TiO₂ electrodes were also investigated by electrochemical impedance spectroscopy. From the cyclic voltammetry data (Figure 5), it was determined that [Fe(CN)₆]^{3−}/[Fe(CN)₆]^{4−} redox reaction potential depends on the film nature. For this reason, for EIS measurements, cathodic peak potential obtained for the film in the presence of a redox probe was chosen and compared with the same film without a redox probe. The obtained data are presented in Nyquist plots (Figure 6). In most cases, two distinct parts can be observed in Nyquist plots—a semicircle in the high-frequency region and the tail in a lower-frequency region. The high-frequency region is related to the overall charge transfer resistance, R_{ct} , between the electrode-electrolyte interface. It was observed that the Nyquist plots of unmodified Ti/TiO₂ and Ti/TiO_x samples do not display a semicircular shape (Figure 6A—filled rhombus and open rhombus; Figure 6B—blue circles), producing a straight line approaching 90 degrees, meaning that impedance at the high and low frequency region is dominated by capacitive behavior of the films. However, TiO_x films in the presence of a redox probe in a high-frequency region exhibit a semicircular shape (Figure 6B orange circles), indicating that the process is limited to charge transfer. Unlike the TiO_x films, an inclined line at 45° in a lower-frequency region was observed on Ti/TiO₂ films in the presence of a redox probe (Figure 6A, open rhombus), showing that the redox reaction displays diffusion limitations, which is referred as a Warburg impedance.

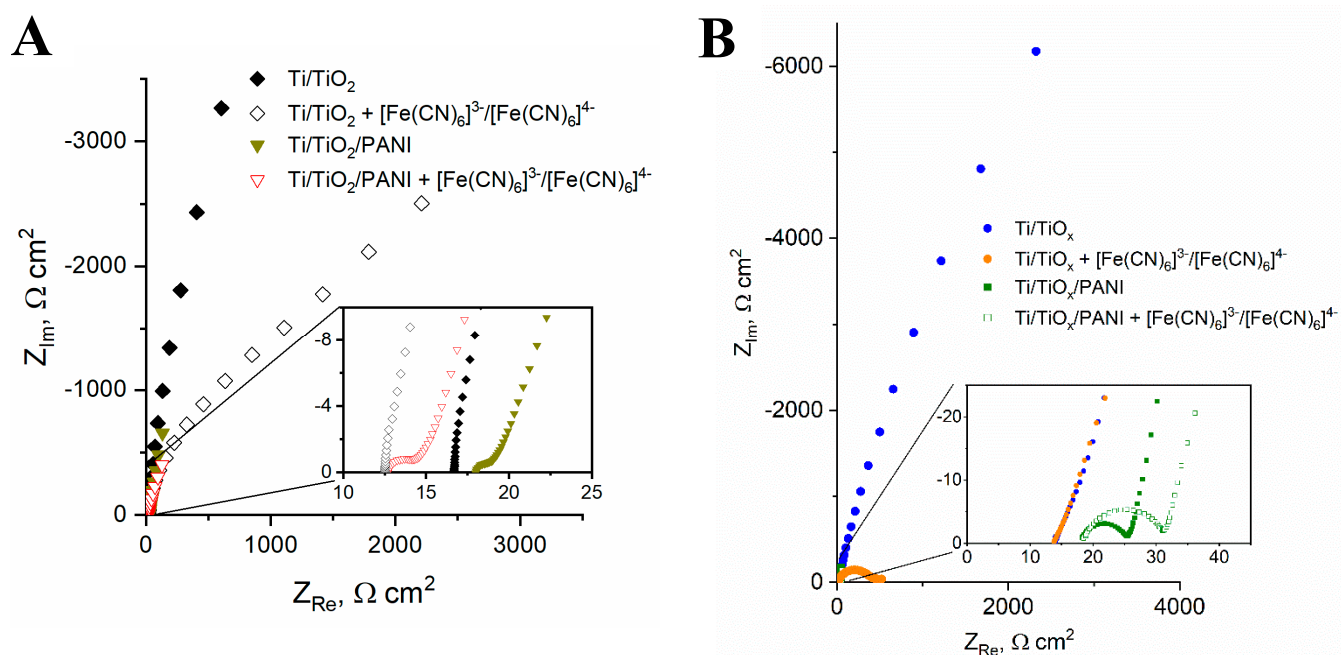


Figure 6. Nyquist plots of Ti/TiO₂, Ti/TiO₂/PANI (A) and TiO_x, TiO_x/PANI (B) with and without 5 mM [Fe(CN)₆]^{3−}/[Fe(CN)₆]^{4−}. Insets: magnification of the spectra.

PANI-decorated films exhibit semi-circular shape in the high frequency range, displaying charge transfer resistance (Figure 6A—open red triangles and filled dark yellow triangles, Figure 6B—red open and filled squares) and different conductive properties. Interestingly, smaller diameters of semicircle were obtained on both films in an absence of a redox probe (Figure 6A—filled dark yellow triangles and Figure 6B—filled green squares), exhibiting smaller charge transfer resistance. Another important characteristic of PANI-decorated film spectra with or without a redox probe is a tail in a lower-frequency region that is vertical and almost parallel to the imaginary impedance axis. Usually, the inclined line in the lower frequency region is related to the porous structure of the electrode [48]. However, the morphology of flowered PANI species deposited onto the nanotubed TiO₂ (Figure 3) differs significantly from the frost-type PANI species (Figure 2) deposited onto the leaflets of TiO_x (Figure 2). Clearly, observed similarities of the inclined line in a lower frequency region of Ti/TiO_x/PANI and Ti/TiO₂/PANI derive from the PANI itself, which indicates capacitive behavior. Such capacitive-like behavior represents an accumulation of diffusion ions in the PANI structure [49,50].

All in all, PANI-decorated substrates exhibited significant difference from unmodified films in electrochemical properties: enhanced conductivity together with electron-transfer kinetics and near-ideal supercapacitive properties.

4. Conclusions

In this research, nanotubed TiO₂ and nano leaflet-shaped TiO_x films possessing different surface morphology were designed and decorated with PANI species by chemical deposition. Based on SEM images, it was established that the surface morphology of titania films greatly affects the morphology of PANI species. The frost-type PANI precipitates were observed on TiO_x nanoleaflets, and flower-like PANI fragments on a nanotubed TiO₂ substrate. Raman spectroscopy suggested that in both cases, PANI films are in the emeraldine base state. We also determined the electrochemical properties of nanotubed TiO₂ and TiO_x films, based on cyclic voltammetry and electrochemical impedance spectroscopy. As expected, both films displayed capacitive behavior and impaired electron-transfer kinetics due to the presence of the oxide layer on the Ti surface. However, samples decorated with

PANI in all cases displayed different electrochemical properties: enhanced conductivity and electron-transfer kinetics, and near-ideal supercapacitive properties.

We suppose that these substrates have an indispensable potential for the development of novel supercapacitors. Nanotubed TiO₂, TiO_x, and PANI are considered to be biocompatible; therefore, the findings in this study could find potential use in bio-organic semiconductors for the detection of relevant biological material. Moreover, based on the low-band gap of TiO_x film, together with PANI decoration, possible applications for supercapacitors or biosensors may be considered.

Author Contributions: T.S.: Methodology, Investigation, Formal analysis, Data curation, Software, Validation, Writing—Review and Editing. S.R.: Investigation, Visualization, Writing—Review and Editing. A.N.: Investigation, Visualization. G.N.: Investigation, Formal analysis, Writing—Original Draft. A.J.: Supervision, Formal analysis, Conceptualization, Writing—Original Draft, Writing—Review and Editing. All authors have read and agreed to the published version of the manuscript.

Funding: This research received no external funding.

Institutional Review Board Statement: Not applicable.

Informed Consent Statement: Not applicable.

Data Availability Statement: Not applicable.

Conflicts of Interest: The authors declare no conflict of interest.

References

1. Geniès, E.; Boyle, A.; Lapkowski, M.; Tsintavis, C. Polyaniline: A historical survey. *Synth. Met.* **1990**, *36*, 139–182. [\[CrossRef\]](#)
2. Mozafari, M.; Chauhan, N.P.S. *Fundamentals and Emerging Applications of Polyaniline*; Elsevier: Amsterdam, The Netherlands, 2019.
3. Zare, E.N.; Makvandi, P.; Ashtari, B.; Rossi, F.; Motahari, A.; Perale, G. Progress in Conductive Polyaniline-Based Nanocomposites for Biomedical Applications: A Review. *J. Med. Chem.* **2020**, *63*, 1–22. [\[CrossRef\]](#) [\[PubMed\]](#)
4. Laourari, I.; Lakhdari, N.; Belgherbi, O.; Medjili, C.; Berkani, M.; Vasseghian, Y.; Golzadeh, N.; Lakhdari, D. Antimicrobial and antifungal properties of NiCu-PANI/PVA quaternary nanocomposite synthesized by chemical oxidative polymerization of polyaniline. *Chemosphere* **2021**, *291*, 132696. [\[CrossRef\]](#)
5. You, C.; Wu, H.; Wang, M.; Wang, S.; Shi, T.; Luo, Y.; Sun, B.; Zhang, X.; Zhu, J. A strategy for photothermal conversion of polymeric nanoparticles by polyaniline for smart control of targeted drug delivery. *Nanotechnology* **2017**, *28*, 165102. [\[CrossRef\]](#)
6. Nandihalli, N.; Liu, C.-J.; Mori, T. Polymer based thermoelectric nanocomposite materials and devices: Fabrication and characteristics. *Nano Energy* **2020**, *78*, 105186. [\[CrossRef\]](#)
7. Xu, D.; Fan, L.; Gao, L.; Xiong, Y.; Wang, Y.; Ye, Q.; Yu, A.; Dai, H.; Yin, Y.; Cai, J.; et al. Micro-Nanostructured Polyaniline Assembled in Cellulose Matrix via Interfacial Polymerization for Applications in Nerve Regeneration. *ACS Appl. Mater. Interfaces* **2016**, *8*, 17090–17097. [\[CrossRef\]](#)
8. Li, M.; Guo, Y.; Wei, Y.; MacDiarmid, A.G.; Lelkes, P.I. Electrospinning polyaniline-contained gelatin nanofibers for tissue engineering applications. *Biomaterials* **2006**, *27*, 2705–2715. [\[CrossRef\]](#)
9. Samukaite-Bubniene, U.; Valiūnienė, A.; Bucinskas, V.; Genys, P.; Ratautaite, V.; Ramanaviciene, A.; Aksun, E.; Tereshchenko, A.; Zeybek, B.; Ramanavicius, A. Towards supercapacitors: Cyclic voltammetry and fast Fourier transform electrochemical impedance spectroscopy based evaluation of polypyrrole electrochemically deposited on the pencil graphite electrode. *Colloids Surf. A Physicochem. Eng. Asp.* **2021**, *610*, 125750. [\[CrossRef\]](#)
10. Viter, R.; Kunene, K.; Genys, P.; Jevdokimovs, D.; Ert, D.; Sutka, A.; Bisetty, K.; Viksna, A.; Ramanaviciene, A.; Ramanavicius, A. Photoelectrochemical Bisphenol S Sensor Based on ZnO-Nanorods Modified by Molecularly Imprinted Polypyrrole. *Macromol. Chem. Phys.* **2019**, *221*, 1900232. [\[CrossRef\]](#)
11. Ratautaite, V.; Brazys, E.; Ramanaviciene, A.; Ramanavicius, A. Electrochemical sensors based on l-tryptophan molecularly imprinted polypyrrole and polyaniline. *J. Electroanal. Chem.* **2022**, *917*, 116389. [\[CrossRef\]](#)
12. Ratautaite, V.; Boguzaitė, R.; Brazys, E.; Ramanaviciene, A.; Ciplys, E.; Juozapaitis, M.; Slibinskas, R.; Bechelany, M.; Ramanavicius, A. Molecularly imprinted polypyrrole based sensor for the detection of SARS-CoV-2 spike glycoprotein. *Electrochim. Acta* **2022**, *403*, 139581. [\[CrossRef\]](#) [\[PubMed\]](#)
13. Bhadra, S.; Khastgir, D.; Singha, N.K.; Lee, J.H. Progress in preparation, processing and applications of polyaniline. *Prog. Polym. Sci.* **2009**, *34*, 783–810. [\[CrossRef\]](#)
14. Mažeikienė, R.; Niaura, G.; Malinauskas, A. A comparative multiwavelength Raman spectroelectrochemical study of polyaniline: A review. *J. Solid State Electrochem.* **2019**, *23*, 1631–1640. [\[CrossRef\]](#)
15. Gicevicius, M.; Kucinski, J.; Ramanaviciene, A.; Ramanavicius, A. Tuning the optical pH sensing properties of polyaniline-based layer by electrochemical copolymerization of aniline with o-phenylenediamine. *Dye. Pigment.* **2019**, *170*, 107457. [\[CrossRef\]](#)

16. Abu-Thabit, N.Y. Chemical Oxidative Polymerization of Polyaniline: A Practical Approach for Preparation of Smart Conductive Textiles. *J. Chem. Educ.* **2016**, *93*, 1606–1611. [\[CrossRef\]](#)
17. Li, Z.; Yang, S.; Song, Y.; Xu, H.; Wang, Z.; Wang, W.; Zhao, Y. Performance evaluation of treating oil-containing restaurant wastewater in microbial fuel cell using in situ graphene/polyaniline modified titanium oxide anode. *Environ. Technol.* **2018**, *41*, 420–429. [\[CrossRef\]](#)
18. Li, Z.; Yang, S.; Song, Y.; Xu, H.; Wang, Z.; Wang, W.; Dang, Z.; Zhao, Y. In-situ modified titanium suboxides with polyaniline/graphene as anode to enhance biovoltage production of microbial fuel cell. *Int. J. Hydrog. Energy* **2019**, *44*, 6862–6870. [\[CrossRef\]](#)
19. Dahl, M.; Liu, Y.; Yin, Y. Composite Titanium Dioxide Nanomaterials. *Chem. Rev.* **2014**, *114*, 9853–9889. [\[CrossRef\]](#)
20. Xu, B.; Sohn, H.Y.; Mohassab, Y.; Lan, Y. Structures, preparation and applications of titanium suboxides. *RSC Adv.* **2016**, *6*, 79706–79722. [\[CrossRef\]](#)
21. Ramanavicius, S.; Tereshchenko, A.; Karpicz, R.; Ratautaite, V.; Bubniene, U.; Maneikis, A.; Jagminas, A.; Ramanavicius, A. TiO_{2-x}/TiO₂-Structure Based ‘Self-Heated’ Sensor for the Determination of Some Reducing Gases. *Sensors* **2019**, *20*, 74. [\[CrossRef\]](#)
22. Ramanavicius, S.; Ramanavicius, A. Insights in the Application of Stoichiometric and Non-Stoichiometric Titanium Oxides for the Design of Sensors for the Determination of Gases and VOCs (TiO_{2-x} and Ti_nO_{2n-1} vs. TiO₂). *Sensors* **2020**, *20*, 6833. [\[CrossRef\]](#) [\[PubMed\]](#)
23. Jagminas, A.; Naujokaitis, A.; Gaigalas, P.; Ramanavičius, S.; Kurtinaitienė, M.; Trusovas, R. Substrate Impact on the Structure and Electrocatalyst Properties of Molybdenum Disulfide for HER from Water. *Metals* **2020**, *10*, 1251. [\[CrossRef\]](#)
24. Kim, G.; Kong, J.; Kim, J.; Kang, H.; Back, H.; Kim, H.; Lee, K. Overcoming the Light-Soaking Problem in Inverted Polymer Solar Cells by Introducing a Heavily Doped Titanium Sub-Oxide Functional Layer. *Adv. Energy Mater.* **2014**, *5*, 1401298. [\[CrossRef\]](#)
25. Verrelli, E.; Tsoukalas, D. Cluster beam synthesis of metal and metal-oxide nanoparticles for emerging memories. *Solid-State Electron.* **2014**, *101*, 95–105. [\[CrossRef\]](#)
26. Singh, A.; Kalra, V. TiO Phase Stabilized into Freestanding Nanofibers as Strong Polysulfide Immobilizer in Li–S Batteries: Evidence for Lewis Acid–Base Interactions. *ACS Appl. Mater. Interfaces* **2018**, *10*, 37937–37947. [\[CrossRef\]](#) [\[PubMed\]](#)
27. Dronov, A.; Gavrilin, I.; Kirilenko, E.; Dronova, D.; Gavrilov, S. Investigation of anodic TiO₂ nanotube composition with high spatial resolution AES and ToF SIMS. *Appl. Surf. Sci.* **2018**, *434*, 148–154. [\[CrossRef\]](#)
28. Mahmood, P.H.; Amiri, O.; Ahmed, S.S.; Hama, J.R. Simple microwave synthesis of TiO₂/NiS₂ nanocomposite and TiO₂/NiS₂/Cu nanocomposite as an efficient visible driven photocatalyst. *Ceram. Int.* **2019**, *45*, 14167–14172. [\[CrossRef\]](#)
29. Wiener, J.; Shahidi, S.; Goba, M. Laser deposition of TiO₂ nanoparticles on glass fabric. *Opt. Laser Technol.* **2012**, *45*, 147–153. [\[CrossRef\]](#)
30. Zhou, B.; Jiang, X.; Liu, Z.; Shen, R.; Rogachev, A.V. Preparation and characterization of TiO₂ thin film by thermal oxidation of sputtered Ti film. *Mater. Sci. Semicond. Process.* **2012**, *16*, 513–519. [\[CrossRef\]](#)
31. Chen, B.T.D.; Dammann, J.F.; Boback, J.L. Nanomaterials. *Chem. Soc. Rev.* **2017**, *44*, 1861. [\[CrossRef\]](#)
32. Chen, X.; Liu, L.; Yu, P.Y.; Mao, S.S. Increasing Solar Absorption for Photocatalysis with Black Hydrogenated Titanium Dioxide Nanocrystals. *Science* **2011**, *331*, 746–750. [\[CrossRef\]](#) [\[PubMed\]](#)
33. Zhu, G.; Shan, Y.; Lin, T.; Zhao, W.; Xu, J.; Tian, Z.; Zhang, H.; Zheng, C.; Huang, F. Hydrogenated blue titania with high solar absorption and greatly improved photocatalysis. *Nanoscale* **2016**, *8*, 4705–4712. [\[CrossRef\]](#) [\[PubMed\]](#)
34. Xu, J.; Tian, Z.; Yin, G.; Lin, T.; Huang, F. Controllable reduced black titania with enhanced photoelectrochemical water splitting performance. *Dalton Trans.* **2016**, *46*, 1047–1051. [\[CrossRef\]](#) [\[PubMed\]](#)
35. Jagminas, A.; Ramanavičius, S.; Jasulaitienė, V.; Šimėnas, M. Hydrothermal synthesis and characterization of nanostructured titanium monoxide films. *RSC Adv.* **2019**, *9*, 40727–40735. [\[CrossRef\]](#) [\[PubMed\]](#)
36. Rahman, K.H.; Kar, A.K. Effect of band gap variation and sensitization process of polyaniline (PANI)-TiO₂ p-n heterojunction photocatalysts on the enhancement of photocatalytic degradation of toxic methylene blue with UV irradiation. *J. Environ. Chem. Eng.* **2020**, *8*, 104181. [\[CrossRef\]](#)
37. Zhao, Y.-N.; Lee, U.; Suh, M.-K.; Kwon, Y.-U. Synthesis and Characterization of Highly Crystalline Anatase Nanowire Arrays. *Bull. Korean Chem. Soc.* **2004**, *25*, 1341–1345.
38. Zárate, R.; Fuentes, S.; Wiff, J.; Fuenzalida, V.; Cabrera, A. Chemical composition and phase identification of sodium titanate nanostructures grown from titania by hydrothermal processing. *J. Phys. Chem. Solids* **2007**, *68*, 628–637. [\[CrossRef\]](#)
39. Jagminas, A.; Balčiūnaitė, A.; Niaura, G.; Tamašauskaitė-Tamašiūnaitė, L. Electrochemical synthesis and characterisation of polyaniline in TiO₂ nanotubes. *Trans. IMF* **2012**, *90*, 311–315. [\[CrossRef\]](#)
40. Morávková, Z.; Dmitrieva, E. Structural changes in polyaniline near the middle oxidation peak studied by in situ Raman spectroelectrochemistry. *J. Raman Spectrosc.* **2017**, *48*, 1229–1234. [\[CrossRef\]](#)
41. Mažeikienė, R.; Niaura, G.; Malinauskas, A. Raman spectroelectrochemical study of polyaniline at UV, blue, and green laser line excitation in solutions of different pH. *Synth. Met.* **2018**, *243*, 97–106. [\[CrossRef\]](#)
42. Mažeikienė, R.; Niaura, G.; Malinauskas, A. Study of deprotonation processes of polyaniline by differential multiwavelength Raman spectroscopy in an electrochemical system. *Chemija* **2019**, *30*, 219–226. [\[CrossRef\]](#)
43. Niaura, G.; Mažeikienė, R.; Malinauskas, A. Structural changes in conducting form of polyaniline upon ring sulfonation as deduced by near infrared resonance Raman spectroscopy. *Synth. Met.* **2004**, *145*, 105–112. [\[CrossRef\]](#)

44. Cochet, M.; Louarn, G.; Quillard, S.; Buisson, J.P.; Lefrant, S. Theoretical and experimental vibrational study of emeraldine in salt form. Part II. *J. Raman Spectrosc.* **2000**, *31*, 1041–1049. [[CrossRef](#)]
45. Šeděnková, I.; Prokeš, J.; Trchová, M.; Stejskal, J. Conformational transition in polyaniline films—Spectroscopic and conductivity studies of ageing. *Polym. Degrad. Stab.* **2008**, *93*, 428–435. [[CrossRef](#)]
46. Yoon, S.-B.; Yoon, E.-H.; Kim, K.-B. Electrochemical properties of leucoemeraldine, emeraldine, and pernigraniline forms of polyaniline/multi-wall carbon nanotube nanocomposites for supercapacitor applications. *J. Power Sources* **2011**, *196*, 10791–10797. [[CrossRef](#)]
47. Li, X.; Rafie, A.; Smolin, Y.Y.; Simotwo, S.; Kalra, V.; Lau, K.K. Engineering conformal nanoporous polyaniline via oxidative chemical vapor deposition and its potential application in supercapacitors. *Chem. Eng. Sci.* **2019**, *194*, 156–164. [[CrossRef](#)]
48. Lasia, A. Modeling of Impedance of Porous Electrodes. In *Modeling and Numerical Simulations*; Springer: Berlin, Germany, 2008; pp. 67–137.
49. Bieńkowski, K.; Strawski, M.; Szklarczyk, M. The determination of the thickness of electrodeposited polymeric films by AFM and electrochemical techniques. *J. Electroanal. Chem.* **2011**, *662*, 196–203. [[CrossRef](#)]
50. Gholivand, M.B.; Heydari, H.; Abdolmaleki, A.; Hosseini, H. Nanostructured CuO/PANI composite as supercapacitor electrode material. *Mater. Sci. Semicond. Process.* **2015**, *30*, 157–161. [[CrossRef](#)]